Int J Adv Manuf Technol (2018) 94:397–413
DOI 10.1007/s00170-017-0898-5

ORIGINAL ARTICLE

Predictive modeling and the effect of process parameters on the hardness and bead characteristics for laser-cladded stainless steel

Mohammad K. Alam[1] · **Ruth Jill Urbanic**[1] · **Navid Nazemi**[2] · **Afsaneh Edrisy**[1]

Received: 11 March 2017 / Accepted: 27 July 2017 / Published online: 11 August 2017

Abstract Laser cladding is a novel additive manufacturing and surface treatment process associated with many interactive process parameters. Using the response surface method with a central composite design, a structured design of experiments approach was chosen to examine the influence of selected process parameters on the bead geometry and hardness for single-track laser-cladded specimens using AISI 420 stainless steel powder on a AISI 1018 substrate. In the present study, robust predictive models for hardness, bead aspect ratio, and wetting angle with the substrate were determined using multiple regression analysis. The geometry and hardness relationships to the process inputs were evaluated using F-statistics from the analysis of variance and compared by utilizing perturbation plots, 3D surface mapping, and contour plots. The highly coupled non-linear relationships are evident from these analyses, but this study revealed that the laser speed has the most significant effect on the bead microhardness and the powder feed rate was found to be the most significant parameter for these bead geometry parameters. The perturbation plots confirmed this sensitivity of those process parameters. This research study gives a guideline for the selection of appropriate process parameters for the laser cladding process to achieve desired hardness and bead geometry.

Keywords Predictive modeling · Laser cladding · Bead geometry · Microhardness · ANOVA

✉ Ruth Jill Urbanic
jurbanic@uwindsor.ca

Mohammad K. Alam
alam117@uwindsor.ca

Navid Nazemi
navid.nazemi@camufacturing.com

Afsaneh Edrisy
edrisy@uwindsor.ca

[1] Department of Mechanical, Automotive, & Materials Engineering, University of Windsor, Windsor, ON N9B 3P4, Canada

[2] CAMufacturing Solutions Inc., 2455 Wyandotte Street W, Windsor, ON N9B 3P4, Canada

1 Introduction

Laser cladding (LC) is one of the potential additive manufacturing (AM) processes for fabricating a metallic near-net shape 3D part, layer by layer directly from the CAD file. Its usage is also growing as a protective coating solution to repair the worn surfaces of engine parts and tools by depositing a high-quality coating. A laser is used as a heat source to melt the depositing metallic powder (or wire) and the outer part of the substrate [1]. A high-power diode laser beam used in this process can be tailored to a variety of industrial applications with a small to big spot size (less than 1 to 7.2 mm) with localized and minimal heat input [2]. The superior mechanical properties of laser-cladded parts and the homogenous metallurgical bond with a low dilution and heat-affected zone (HAZ) in the substrate make the LC technology an attractive process for both cladding and AM.

The mechanical and physical properties of laser-cladded parts are partially dependent on the process parameters associated with the LC process, and they are largely unknown. Understanding these relationships is essential in developing robust process solutions which are minimally affected by the external sources of variability [3].

As summarized in Table 1, the main process parameters explored by researchers include (but are not limited to): the laser power (LP), the powder feed rate (FR), the laser scanning speed (LS), the lens focal length (FL), and the distance

Table 1 Summary of literature review

Author reference	Materials/process	DOE strategy	Expt. factors	Output variable
Farahmand et al. [2]	H13/LC	RSM/CCD	LP, FR, LS	Bead geometry, hardness
Yuwen Sun et al. [5]	Ti6Al4V/LC	RSM/CCD	LP, FR, LS	Bead geometry
Onwubolu et al. [9]	Diamalloy'02/LC	RSM	LP, FR, LS	clad angle
Shuang Liu et al. [10]	Fe-based alloy (CrMoNiCFe)/LC	RSM/CCD	LP, FR, CGFR, SOD	Powder catchment efficiency, clad geometry
Hyoung Lee [17]	Co alloy powder/LC	Taguchi	SGT, LPS, FR, LS, PFA, PFP, FP	Deposition efficiency
Benjamin Graf et al. [18]	René 80 (Ni)/LC	Full factorial	LP, SD, LS, FR	Bead geometry
Urbanic et al. [6, 8, 12]	420 St. steel/LC	RSM/CCD	FR, LP, FL, LS, CTD	Bead geometry
Mondal et al. [13]	NiCrMo Alloy/LC	Taguchi	FR, LP, LS	Bead Geometry

LC laser cladding, *DOE* design of experiments, *RSM* response surface methodology, *CCD* central composite design, *CTD* contact tip to workpiece distance, *CGFR* carrier gas flow rate, *FR* powder feed rate, *FL* focal length of the Lens, *FP* focal position of a laser beam, *LP* laser power, *LS* laser speed, *LPS* laser pulse shape, *PFA* powder feed angle, *PFP* powder feed position, *SD* spot diameter, *SGT* shielding gas type, *SOD* stand-off distance

between the contact tip to the workpiece (CTD). Additional input parameters, such as the powder grain sizes, surface normal to torch angle, etc. are described in Urbanic et al. [4]. Several experimental design methodologies [2, 5–16] are proposed by researchers to examine the statistical relationships between the process parameters and their impact on the bead geometries and mechanical properties. Those researchers have reported the use of design of experiments and process parameters optimization using full factorial design, Taguchi design, and the response surface method (RSM) with a central composite design.

Parisa Farahmand and Radovan Kovacevic [2] used a central composite design (CCD) with the RSM for the multi-objective optimization for cladding with AISI H13 using the process parameters LP, FR, and LS on the clad bead geometry and clad microhardness. They found that the FR and LS had a significant effect on the clad height, the heat affected zone (HAZ) depth, and the clad microhardness.

Yuwen Sun et al. [5] employed the CCD and RSM to build a mathematical model. They examined the influence of the LP, LS, and FR on the cladding-bead geometry of Ti6Al4V cladding on a TC4 substrate, but they did not assess hardness. They used the ANOVA method to establish relationships between the process parameters and the output responses. Their analysis indicated that the FR had a significant effect on the width and height of cladding coating, while LS had the most significant effect on the penetration depth.

Shuang Liu and Radovan Kovacevic [10] investigated the effects of the main processing parameters such as the LP, FR, the carrier gas flow rate, and the stand-off distance on the output results of powder catchment efficiency and the clad geometry. They also used the RSM with a CCD to find out the statistical relationships and optimal processing parameters. They found that the carrier gas flow rate had the most significant effect on the powder catchment efficiency. The FR, carrier gas flow rate, and interaction of the carrier gas and stand-off distance were the most significant factors affecting the clad height, while the LP was the most effective factor affecting the clad width.

Hyoung-Keun Lee [17] used the Taguchi Method to maximize the deposition efficiency in the cladding of Co alloy powder. He found that the powder feed position had the most significant effect on the deposition efficiency. Graf et al. [18] used a full-factorial design to determine the effect of process parameters on the bead geometry of laser metal deposition of a Nickel-based superalloy René 80. Saqib et al. [6], Urbanic et al. [8], and Aggarwal et al. [12] performed similar analyses using RSM and CCD along with an artificial neural network to establish statistical model and relationship between bead geometry (width, height, penetration, and dilution) and the main process parameters for laser-cladded AISI 420 stainless steel. The present study used all five process parameters including the FL and CTD, which are shown in Fig. 1.

Most of the researchers have focused on the bead geometry when developing predictive models. However, two important characteristics of bead geometry, namely the aspect ratio of the bead (width-to-height ratio and depth of penetration to bead width ratio) and the bead wetting angle, have not been investigated. Also, there is a lack of research on the statistical relationships between the process parameters and the bead microhardness. The clad geometry functional characteristics must be considered in tandem with the bead geometry for effective process planning solutions. The current authors investigated [19] predictive modeling approaches for microhardness by using a simple multiple regression for a narrow set of parameters and experimental settings by perturbing one factor at a time around a central set point. However, the model was not expandable for a wide range of process parameter settings. For process planning, quadratic models need to be developed for the large set of variables involved in the laser cladding process.

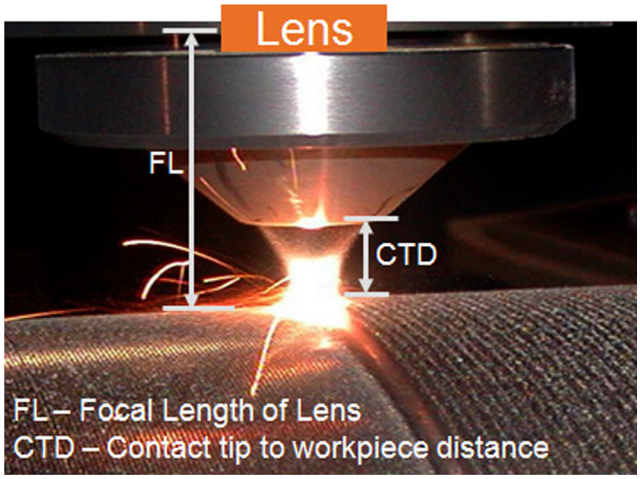

Fig. 1 Laser cladding

The present research targets laser-cladded AISI 420 stainless steel for single-track beads. The application of 420 stainless steel is increasing as one of the potential alloys for laser cladding additive fabrication. Unlike other stainless steels, the properties of this stainless steel can be changed by heat treatment [20]. Hence, these steels are generally used for a wide range of applications such as steam generators, pressure vessels, mixer blades, cutting tools, and medical applications. Moreover, it provides excellent wear resistance and high surface hardness required for the die and tool repair when coated by laser cladding [21].

In this paper, the RSM is applied using the CCD to establish the experimental conditions. *F*-statistics from the analysis of variance (ANOVA), perturbation plotting, surface mapping, and contour plotting methods are employed to investigate the statistical correlations among the process parameters, bead geometry, and the bead microhardness. Quantitative and qualitative analyses are performed to illustrate the non-linear influence of the laser cladding process. The long-term goal of this research is to develop process planning strategies for the additive manufacturing process to fabricate a component with the desired geometry and physical characteristics. This research will help to predict the bead aspect ratio as the width can be easily measured (i.e., with a camera control system), while functional characteristics such as hardness can easily be correlated to the strength of laser-cladded AISI 420 stainless steel [22, 23].

2 Research methodology

The methodology for the experimentation strategy, data collection, and simulations is presented in this section. The process flow for the overall research plan is illustrated in Fig. 2, showing the various experimentation, simulation, and analysis aspects. This paper focuses on the statistical analyses elements, which are presented in section 3.

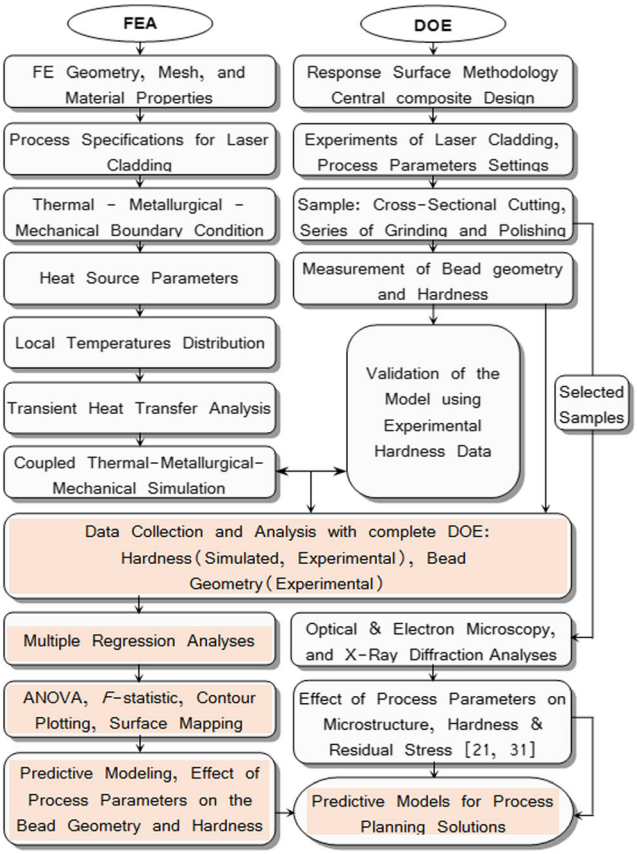

Fig. 2 Procedure of the experimentation, simulation, validation, and research outputs

2.1 Design of Experiments (DOE)

The statistical software Design-Expert Version 10 was employed to configure the experiments using the response surface methodology with a CCD. It is hypothesized that the CCD approach can provide the necessary information related to the process parameters and their interactions on the response variables (e.g., microhardness, bead geometry) over a wide range of process settings. This design approach is also readily expandable, if necessary. A five-factor, five-level design matrix was established at a half fraction and an alpha value of 2, with 3 replicates of the factorial and the axial points, and 18 replicated central points. The CCD approach provides 96 experimental runs (18 central points and 78 non-central points) in contrast to a full-factorial DOE approach, which would require 5^5 experiments [24]. The experimental configuration and codes are shown in Table 2.

2.2 Laser cladding experiments

The experiments were performed at an industrial facility using a 4-kW fiber diode laser coupled to an articulated robotic arm, on a 6.4-mm flat bar of medium carbon steel substrate. The

Table 2 Process parameters and coding

Factors	Units	Notations	Coding and values of Factors				
			−2	−1	0	1	2
Powder feed rate (FR)	gm/min	FR	10	15	20	25	30
Laser power (LP)	kW	LP	1	2	2.5	3	4
Focal length of lens (FL)	mm	FL	380	390	400	410	420
Laser speed (LS)	mm/s	LS	5	7.5	10	12.5	15
Contact tip to workpiece distance (CTD)	mm	CTD	21	22	23	24	25

powder density of the stainless steel was 4.37 g/cm^3 with a 53–180 μm grain size [21]. The chemical composition of the alloy powder is shown in Table 3.

A high-power laser beam was focused on the substrate materials to generate a molten pool, while the AISI 420 stainless steel metal powder was injected simultaneously into the focal area of the laser through coaxial nozzles with flowing argon gas. The argon gas serves as a shield to protect the molten pool from oxidation. A series of the single beads were cladded on the substrate with different processing parameters (Table 2) [21].

2.3 Light optical microscopy and measurement of bead geometry

The metallographic work such as grinding and polishing of the cross-sectional samples was done manually as per the Struers application notes for the stainless steel materials [25]. The microscopy observations were made using a Leica Q5501W light microscope. The bead width, height, and depth of penetration were measured using Image-Pro Plus software as per the bead geometry shown in Fig. 3a. The bead width-to-height ratio, the penetration depth-to-the bead width ratio, and the bead wetting angle are calculated based on the measured bead geometry.

2.4 Measurement of bead microhardness

A Buehler microhardness tester was used to measure the bead microhardness (Vickers) using a load of 200 g and a loading time of 12 s. The measurements were performed at the center of the bead at a 100-μm interval from the top of the bead, and through the dilution and HAZ, and part of the substrate materials. Two measurements were performed at a 250-μm distance, from each side of the first indentation set (Fig. 3a) [21]. The average hardness values were measured from these three measurements. This generated 5–8 values per bead. This set of averaged hardness values from the center line is used to generate a baseline set for the finite element analysis (FEA) simulation models. This experimental microhardness data is collected from a selected set of experiments. The balance of the data is generated from simulation results, as the FEA model results correlate well to the collected hardness data.

2.5 Simulation of bead microhardness

The LC simulation was performed with the finite element (FE) software, SYSWELD. This simulation solution considers the variable thermal and mechanical properties of the cladded and substrate materials along with the metallurgical reactions. The nodal temperatures and phase transformations are calculated in a coupled thermal-metallurgical-mechanical analysis. The thermo-physical properties depend on the temperature and the metallurgical proportions of each phase. Information on the heat source, boundary conditions, governing thermal equations, mesh, and convergent studies for the simulation and the model goodness of fit for single and overlapping beads are provided in the current authors' earlier study [26–28]. Similar analytical model of laser cladding by power injection is also found in the study of Toyserkani et al. [29] and Fu. Y. et al. [30].

Experimental hardness data from a wide variety of bead shapes are used to validate the model. Figure 1b depicts the simulated hardness variation data from the top of the bead to the HAZ in the substrate. The simulation hardness data and the experimental data are found to have a good agreement

Table 3 Chemical composition of the cladding powder (420 stainless steel)

Chemical elements	Percentage of composition (%)
Carbon	0.23
Manganese	1.2
Chromium	12.6
Silicon	0.5
Iron	Balance
Cobalt	0.02

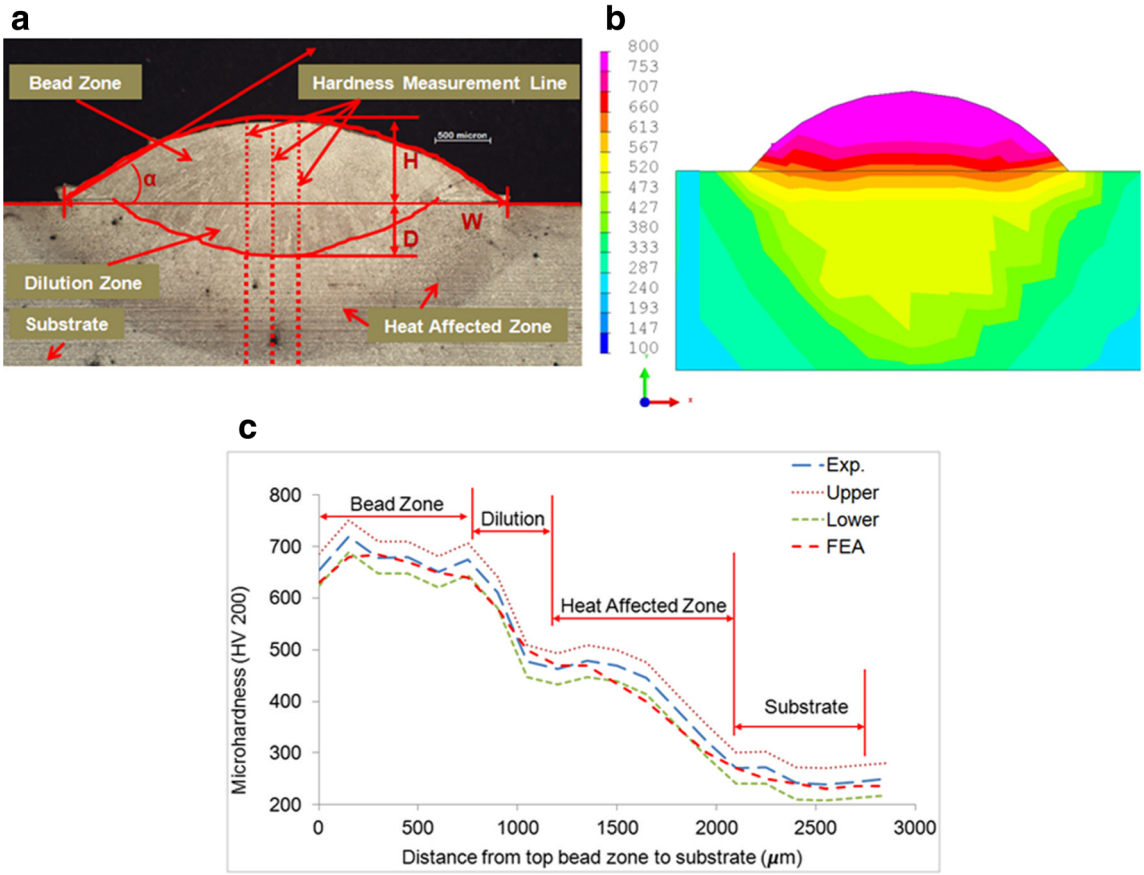

Fig. 3 **a** A cross-sectional bead sample showing the bead geometry (*W* width, *H* height, *D* depth of penetration, α wetting angle), dilution zone (diffusion between clad and substrate), heat affected zone, substrate, and the hardness measurement lines. **b** FEA model for a single bead laser cladded sample. **c** Comparison of hardness profile of experimental results with the simulated result for a single bead sample

(Fig. 1c); consequently, simulation data is used along with the average measured hardness values.

2.6 Predictive modeling

The experimental and simulation data are utilized to develop statistical-based predictive models. The analysis of variance (ANOVA) technique was utilized for finding the statistically significant process parameters and their interactions. To develop the relationship between various processing parameters and the corresponding response variables, a second-order regression model was used to fit the experimental data, as described in Eq. (1):

$$y = \beta_0 + \sum_{j=1}^{k} \beta_j x_j + \sum_{i,j=1}^{k} \beta_{ij} x_i x_j + \sum_{j=1}^{k} \beta_{jj} x_j^2 + \epsilon \quad \ldots\ldots\ldots\ldots\ldots\ldots\ldots\ldots\ldots\ldots \quad (1)$$

Where y is the predicted response value for this quadratic model with β_0 as the y-intercept and βj, βij, and βjj are the regression coefficient of linear, interaction, and quadratic terms; xj is the processing parameter; k is the number of factors; and ε is the associated error.

When considering the effects of five process parameters associated with the LC process, Eq. (1) can be re-written as:

$$\begin{aligned} y = {} & \beta_0 + \beta_1{}^{*}\mathrm{FR} + \beta_2{}^{*}\mathrm{LP} + \beta_3{}^{*}\mathrm{FL} + \beta_4{}^{*}\mathrm{LS} + \beta_5{}^{*}CTD \\ & + \beta_{12}{}^{*}\mathrm{FR}{}^{*}\mathrm{LP} + \beta_{13}{}^{*}\mathrm{FR}{}^{*}\mathrm{FL} + \beta_{14}{}^{*}\mathrm{FR}{}^{*}\mathrm{LS} + \beta_{15}{}^{*}\mathrm{FR}{}^{*}\mathrm{CTD} \\ & + \beta_{23}{}^{*}\mathrm{LP}{}^{*}\mathrm{FL} + \beta_{24}{}^{*}\mathrm{LP}{}^{*}\mathrm{LS} + \beta_{25}{}^{*}\mathrm{LP}{}^{*}\mathrm{CTD} + \beta_{34}{}^{*}\mathrm{FL}{}^{*}\mathrm{LS} \\ & + \beta_{35}{}^{*}\mathrm{FL}{}^{*}\mathrm{CTD} + \beta_{45}{}^{*}\mathrm{LS}{}^{*}\mathrm{CTD} + \beta_{11}{}^{*}(\mathrm{FR})^2 + \beta_{22}{}^{*}(\mathrm{LP})^2 \\ & + \beta_{33}{}^{*}(\mathrm{FL})^2 + \beta_{44}{}^{*}(\mathrm{LS})^2 + \beta_{55}(\mathrm{CTD})^2 \ldots\ldots\ldots\ldots\ldots\ldots\ldots \end{aligned} \quad (2)$$

Where.

FR	Power feed rate
LP	Laser power
FL	Focal length of lens
LS	Laser speed
CTD	Contact tip to workpiece distance

The multiple regression results were utilized to predict the optimal settings and to create a final model equation for the respective responses as per Eq. 2.

Table 4 Analysis of variance (ANOVA) results for multiple responses

Model	Sum of squares (SS)		Degree of freedom (df)		Mean square (MS)		F value	*p* value	R-squared value	Adj. R-Sqd. value	Pred. R-Sqd. value
Responses	Regression	Residuals	Regression	Residuals	Regression	Residuals		Prob > F			
Bead W/H ratio	215.79	17.2	20.0	69.0	10.79	0.25	43.4	0.0001	0.93	0.90	0.88
Bead D/W ratio	0.22	0.02	20.0	69.0	0.01	2.6×10^4	42.2	0.0001	0.92	0.90	0.87
Bead wetting angle	2514.93	270.02	20.0	69.0	125.8	3.91	32.1	0.0001	0.90	0.87	0.85
Bead microhardness	3.6×10^5	18,823.5	20.0	69.0	18,000	272.80	66.0	0.0001	0.95	0.94	0.92

3 Results and discussions

3.1 Multiples regression analysis

The ANOVA method was used to trace the significant process parameters and their interactions effect on the predicted responses. The key results for the ANOVA outcomes are presented in Table 4. The overall regression model for bead W/H ratio, bead D/W ratio, bead angle, and bead microhardness are found to be significant with an *F*-value of 43.36, 41.17, 32.13, and 65.98, respectively, with a *P* value of 0.0001. There is only a 0.01% chance that such a large *F* value could occur due to noise. Usually, values of "Prob > F" being less than 0.05 indicate that the model terms are significant at a 95% confidence level [31].

The R-squared values for all the models are between 0.90 and 0.95 (Table 4). This means approximately 90–95% of the variability of the response values are accounted for with Eq. (2). However, to understand how close these data are fitted to the regression line or how well the quadratic model fits those set of observations, two additional types of R-squared values are calculated: the Adjusted R-squared (between 0.87 and 0.94) and predicted R-squared values (between 0.85–0.91). Both sets of values are in reasonable agreement with each other as the differences between each set of adjusted and predicted R-squared values is less than 0.2 [31]. It is to be noted that the adjusted R-squared provides an unbiased estimate of the population R-squared.

Table 5 summarizes the most significant factors in the predictive models. Figure 4 illustrates the significance of the process parameters (linear term) on the predictive responses as per their rank based on the *F*-statistics. It is revealed that the FR is the most significant process parameter for the bead aspect ratio and wetting angle, while LS is most significant for the bead microhardness. Similar observations were reported by Farahmand et al. [2] and Yuwen Sun et al. [5]. Though the FL is the most insignificant process parameter for the bead geometric characteristics, it has a significant effect on the bead microhardness. Most interestingly, the LP is found to be less significant despite being a prime input for melting the alloy powder and substrate. It is believed to be due to fact that the melt pool saturation temperature could be attained at a much

Table 5 Most significant factors on the bead geometry and bead microhardness

Most significant factors on the bead geometry and bead microhardness (Based on ANOVA, *F* statistics)

Ranking # parameters	Bead geometry									Bead microhardness		
	w/h ratio			D/W ratio			Wetting angle					
	Linear	Interaction	Quadratic	Linear	Interaction	Quadratic	Linear	Interaction	Quadratic	Linear	Interaction	Quadratic
1	FR	FR*LS	FR^2	FR	FR*LS	FR^2	FR	FR*LP	FR^2	*LS*	FR**LS*	CTD^2
2	LS	FL*CTD	CTD^2	LS	FL*CTD	CTD^2	LS	FL*CTD	CTD^2	FL	LP*FL	LS^2
3	CTD	LS*CTD	LS^2	CTD	LS*CTD	LS^2	LP	LS*CTD	LP^2	FR	LP*CTD	LP^2
4	LP	FR*LP	LP^2	LP	FR*LP	LP^2	CTD	LP*LS	LS^2	LP	FL*CTD	FL^2
5	-	FL*LS	FL^2	–	FL*LS	FL^2	–	–	FL^2	CTD	FL*LS	FR^2

FR powder feed rate, *LP* laser power, *LS* laser speed, *CTD* contact tip to workpiece distance, *FL* focal length of lens, *W/H* width-to-height ratio, *D/W* depth of penetration-to-width ratio

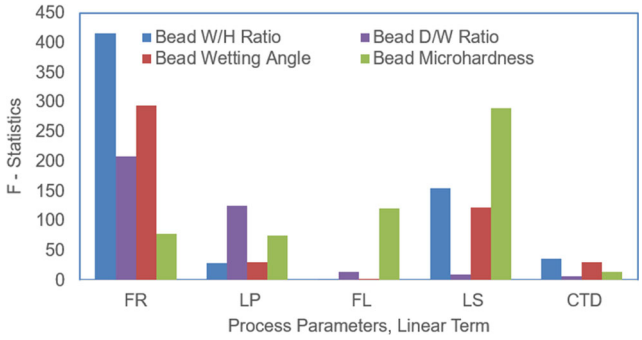

Fig. 4 Significance of process parameters on the predicted Bead geometry and bead microhardness

lower range of power (1000–2500 W). Therefore, more than 2500 kW of LP is a waste and does not have any significant effect [19]. More details on the individual effect of those process parameters and their interactions are discussed in Section 3.2.1.

3.1.1 Development of predictive models

Based on the coefficient estimates of RSM multiple regression shown in Table 6, the final regression equation for the predictive models of the bead W/H ratio, D/W ratio, bead wetting angle, and bead microhardness are expressed in Eqs. 3, 4, 5, and 6. These regression coefficients represent the expected change in response variables per unit change in factors when all remaining factors are held constant. The coefficients for each of the factors indicate the amount of change one could expect in the response output given a one-unit change in the value of that factor at a constant value for all other factors in the model. For example, if FR is considered as a factor, then an increase of 18.51 in the microhardness value for every one-unit increase in FR is expected, keeping all other factors in the model Eq. 6 constant.

$$\begin{aligned} Bead\frac{W}{H}Ratio = {} & 4.08 - 1.2^{*}FR + 0.38^{*}LP - 0.075^{*}FL + 0.73^{*}LS \\ & + 0.35^{*}CTD + 0.15^{*}FR^{*}LP - 0.083^{*}FR^{*}FL \\ & - 0.5^{*}FR^{*}LS + 0.033^{*}FR^{*}CTD - 0.094^{*}LP^{*}FL \\ & - 0.1^{*}LP^{*}LS + 0.13^{*}LP^{*}CTD + 0.15^{*}FL^{*}LS \\ & - 0.22^{*}FL^{*}CTD - 0.15^{*}LS^{*}CTD + 0.53^{*}(\mathrm{FR})^{2} \\ & + 0.28^{*}(\mathrm{LP})^{2} + 0.19^{*}(\mathrm{FL})^{2} + 0.23^{*}(\mathrm{LS})^{2} \\ & + 0.28^{*}(\mathrm{CTD})^{2} \end{aligned} \quad (3)$$

Table 6 Estimated coefficients for complete quadratic models

Coefficients estimate	Response outputs			
	Bead W/H ratio	Bead D/W ratio	Bead wetting angle	Bead microhardness
Intercept	4.08	0.0870	26.3	615.53
β_1	−1.2	−0.0280	4	17.14
β_2	0.38	0.0420	−1.5	20.19
β_3	−0.075	−0.0019	0.15	25.61
β_4	0.73	−0.0210	−2.62	33.14
β_5	0.35	−0.0023	−1.26	7.08
β_{12}	0.15	−0.0016	−1.04	8.58
β_{13}	−0.083	0.0025	0.12	13.25
β_{14}	−0.5	0.0086	0.51	−16.67
β_{15}	0.033	−0.0029	−0.45	5.46
β_{23}	−0.094	−0.0050	0.43	−15.83
β_{24}	−0.1	−0.0014	0.87	−0.83
β_{25}	0.13	−0.0070	−0.45	15.46
β_{34}	0.15	−0.0014	−0.51	14.08
β_{35}	−0.22	−0.0035	0.94	−15.21
β_{45}	−0.15	0.0062	0.89	−11.46
β_{11}	0.53	0.0030	−1.27	8.13
β_{22}	0.28	0.0061	−1.2	−19.11
β_{33}	0.19	−0.0037	−0.69	19.01
β_{44}	0.23	0.0039	−0.75	17.8
β_{55}	0.28	0.0044	−1.25	31.76

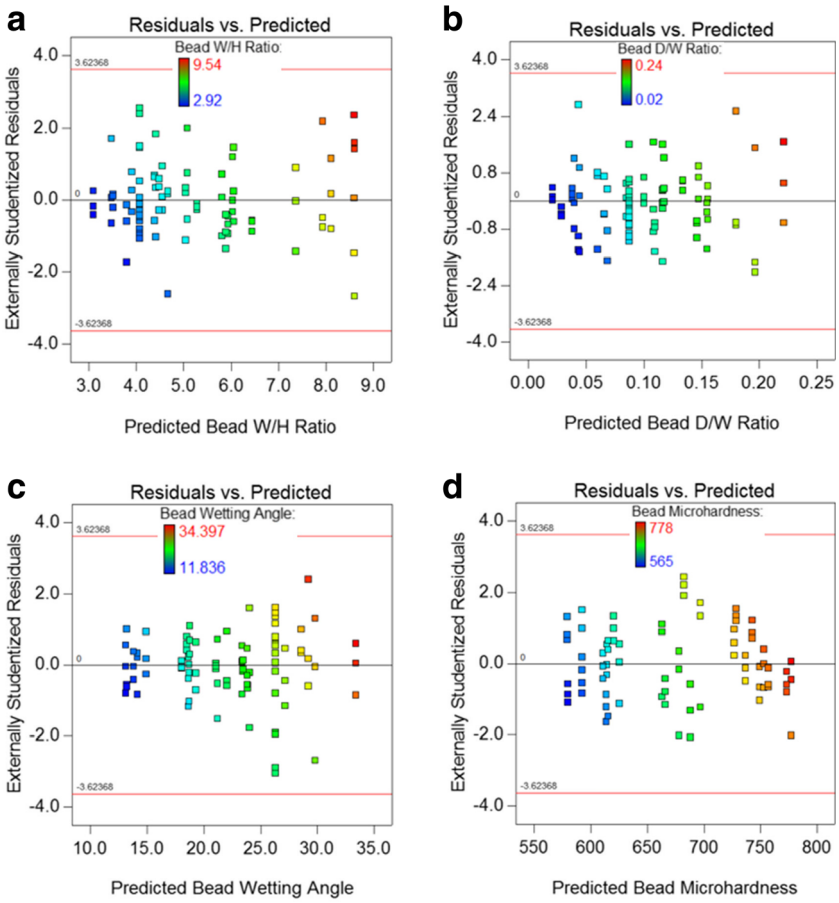

Fig. 5 Residual vs. predicted value of data points

$$\begin{aligned} Bead\ \frac{D}{W}Ratio = {} & 0.087 - 0.028^{*}FR + 0.042^{*}LP - 1.9 \times 10^{-3^{*}}FL \\ & - 0.021^{*}LS - 2.35 \times 10^{-3^{*}}CTD - 1.59 \times 10^{-3^{*}}FR^{*}LP \\ & + 2.55 \times 10^{-3^{*}}FR^{*}FL + 8.61 \times 10^{-3^{*}}FR^{*}LS - 2.89 \\ & \times 10^{-3^{*}}FR^{*}CTD - 5.04 \times 10^{-3^{*}}LP^{*}FL - 1.38 \\ & \times 10^{-3^{*}}LP^{*}LS - 7.0 \times 10^{-3^{*}}LP^{*}CTD - 1.44 \\ & \times 10^{-3^{*}}FL^{*}LS - 3.46 \times 10^{-3^{*}}FL^{*}CTD + 6.23 \\ & \times 10^{-3^{*}}LS^{*}CTD + 3.02 \times 10^{-3^{*}}(\mathrm{FR})^{2} + 6.1 \\ & \times 10^{-3^{*}}(\mathrm{LP})^{2} - 3.74 \times 10^{-3^{*}}(\mathrm{FL})^{2} + 3.89 \\ & \times 10^{-3^{*}}(\mathrm{LS})^{2} + 4.37 \times 10^{-3^{*}}(\mathrm{CTD})^{2} \end{aligned} \quad (4)$$

$$\begin{aligned} Bead\ Wetting\ Angle = {} & 26.3 + 4.0^{*}FR - 1.5^{*}LP + 0.15^{*}FL \\ & - 2.62^{*}LS - 1.26^{*}CTD - 1.04^{*}FR^{*}LP \\ & + 0.12^{*}FR^{*}FL + 0.51^{*}FR^{*}LS - 0.45^{*}FR^{*}CTD \\ & + 0.43^{*}LP^{*}FL + 0.87^{*}LP^{*}LS - 0.45^{*}LP^{*}CTD \\ & - 0.51^{*}FL^{*}LS + 0.94^{*}FL^{*}CTD + 0.89^{*}LS^{*}CTD \\ & - 1.27^{*}(\mathrm{FR})^{2} - 1.2^{*}(\mathrm{LP})^{2} - 0.69^{*}(\mathrm{FL})^{2} \\ & - 0.75^{*}(\mathrm{LS})^{2} - 1.25^{*}(\mathrm{CTD})^{2} \end{aligned} \quad (5)$$

$$\begin{aligned} Microhardness = {} & 620.36 + 18.51^{*}FR + 2.88^{*}LP + 23.85^{*}FL \\ & + 31.76^{*}LS + 8.46^{*}CTD + 10.65^{*}FR^{*}LP \\ & + 11.19^{*}FR^{*}FL - 18.73^{*}FR^{*}LS + 7.52^{*}FR^{*}CTD \\ & - 17.90^{*}LP^{*}FL - 2.90^{*}LP^{*}LS + 17.52^{*}LP^{*}CTD \\ & + 16.15^{*}FL^{*}LS - 17.27^{*}FL^{*}CTD - 13.52^{*}LS^{*}CTD \\ & + 3.31^{*}(\mathrm{FR})^{2} + 4.10^{*}(\mathrm{LP})^{2} + 14.77^{*}(\mathrm{FL})^{2} \\ & + 12.97^{*}(\mathrm{LS})^{2} + 26.93^{*}(\mathrm{CTD})^{2} \end{aligned} \quad (6)$$

Where.

FR	Power feed rate
LP	Laser power
FL	Focal length of lens
LS	Laser speed
CTD	Contact tip to workpiece distance

3.1.2 Validation of the developed models

Figure 5 shows the residuals vs. predicted values of the multiple regression for all models. There is no strong curvature or clusters or unequal variation observed in the distribution of

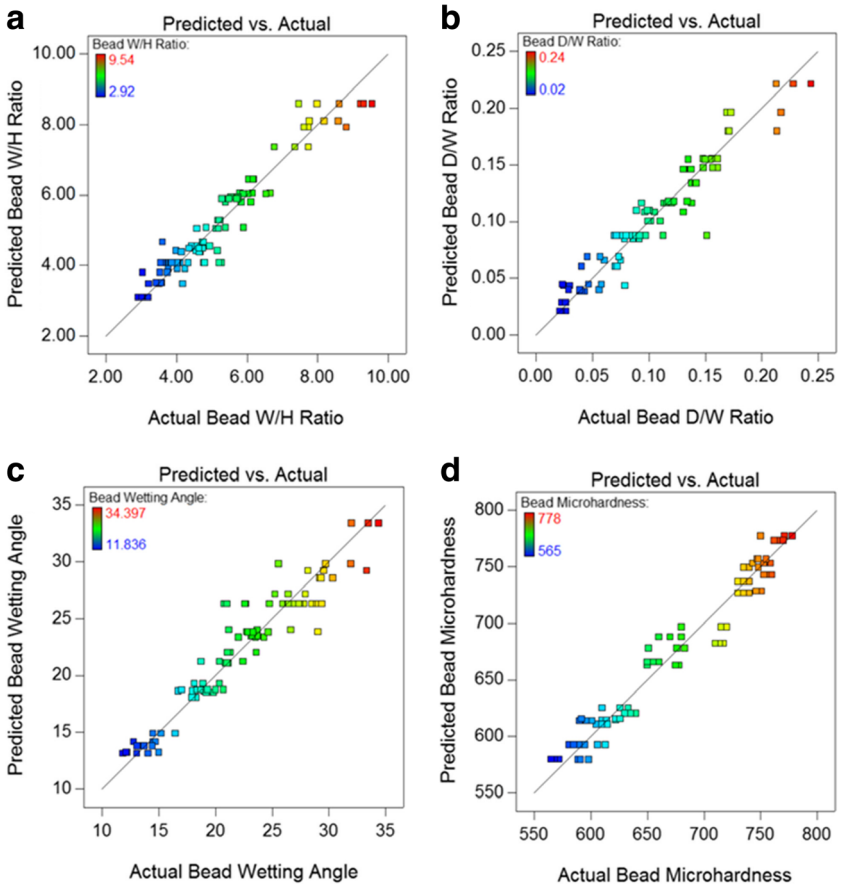

Fig. 6 Actual value vs. predicted value of microhardness

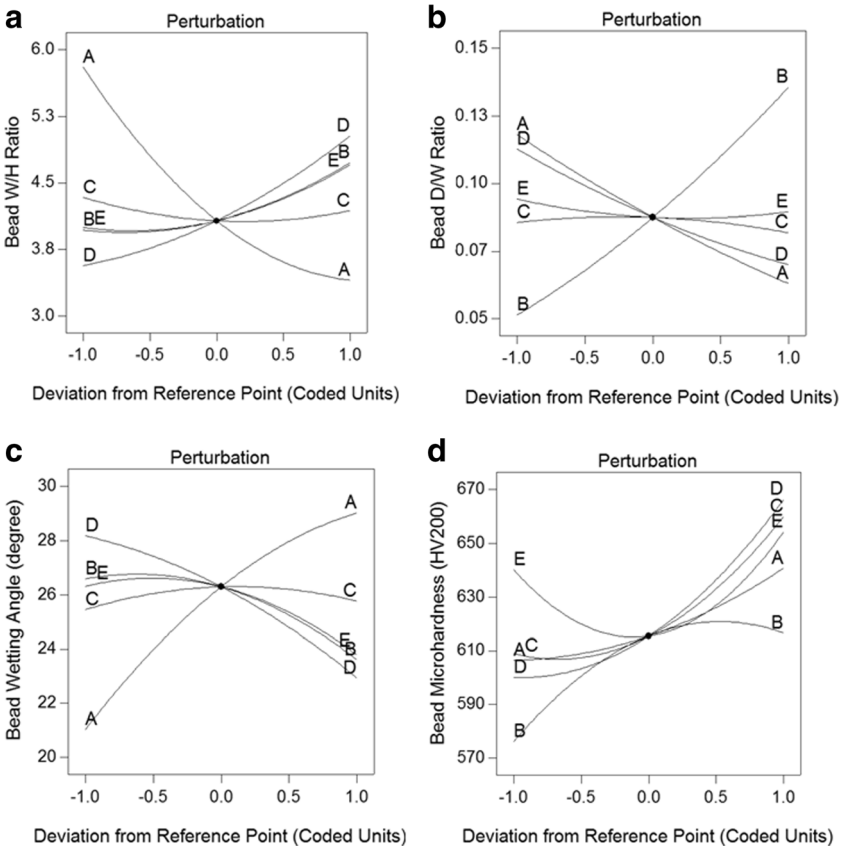

Fig. 7 Perturbation plots showing the effect of all processing parameters on the predicted responses. (curves AA, BB, CC, DD, and EE represent FR, LP, FL, LS, and CTD, respectively)

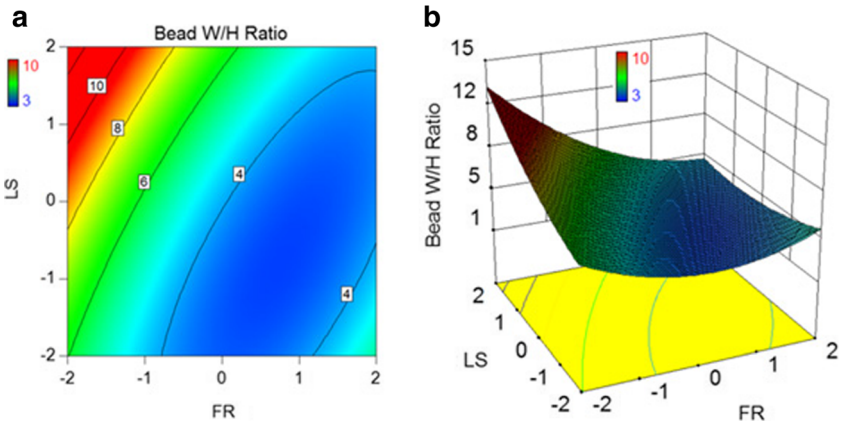

Fig. 8 **a** 2D contour plot and **b** 3D response surface plot show the interaction effect of powder flow rate (*FR*) and laser speed (*LS*) on the bead width to height ratio

data that may indicate problems with the regression models. Data points fall randomly on both sides of the zero line. No outlier residuals are observed outside of the two red lines. This indicates that there is no problem with the residuals and predicted responses. Since the number of data points was large and the residuals are normally distributed, the significant relationship between the process parameters and the output responses indicated by the *p* value is accurate.

Based on Eqs. 3–6, the predicted value of the bead W/H ratio, D/W ratio, bead wetting angle, and bead microhardness are calculated for the coded value of the process parameters and depicted in Fig. 6. These graphs illustrate that the models are well fitted with the experimental and regression results. For instance, 100% of the predicted microhardness values are found within a 0 ± 4% error, where 80% response is within a 0 ± 2% error. Similarly, 83% of the predicted response of bead aspect ratio is found to be within a ± 10% error.

3.2 Relative effects of the process parameters on the predictive responses

The determination of the relative effects of the process variables is an important aspect of multiple regression analysis. The relative importance and the relative effects of the main process parameters (factors) and their interactions are ranked based on their respective *F*-statistics (Table 5). Since *F*-statistics measures the variations of the sum of squares, more variations come from the more sensitive or more significant factors [32]. However, *F*-statistics cannot illustrate the effect of individual process parameters and their interaction on the response outputs. Therefore, perturbation plots are created to explain the relative effect of the individual process parameters, while 2D contour plots and 3D surface plots are created to explain the interactions of those process parameters on the response outputs.

3.2.1 Individual effect analyses

Figure 4 illustrates the relative importance and significance level of the individual process parameters on the respective predictive responses. However, their detailed effects are illustrated by the perturbation plots shown in Fig. 7. These plots also compare the significant effects of all the factors at a particular point in the design space for their respective models. The predicted responses are plotted against the coded factors by changing only one factor over its range while holding all the other factors constant. The reference point is set to the experimental configuration midpoint.

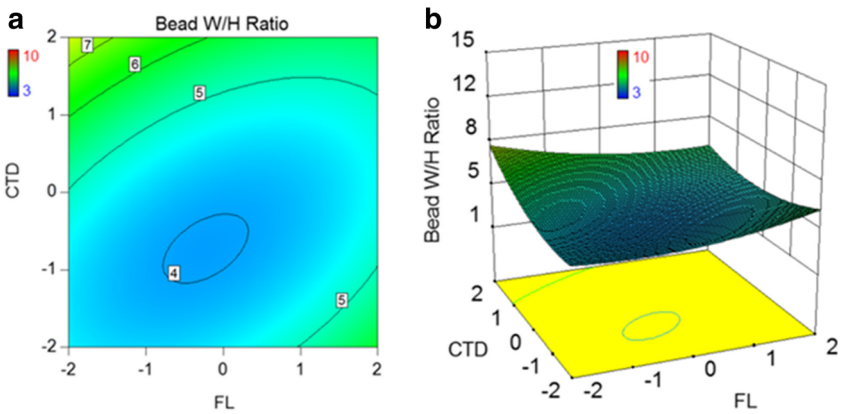

Fig. 9 **a** 2D contour plot and **b** 3D response surface plot show the interaction effect of focal length of the lens (*FL*) and contact tip to workpiece distance (*CTD*) on the bead width-to-height ratio

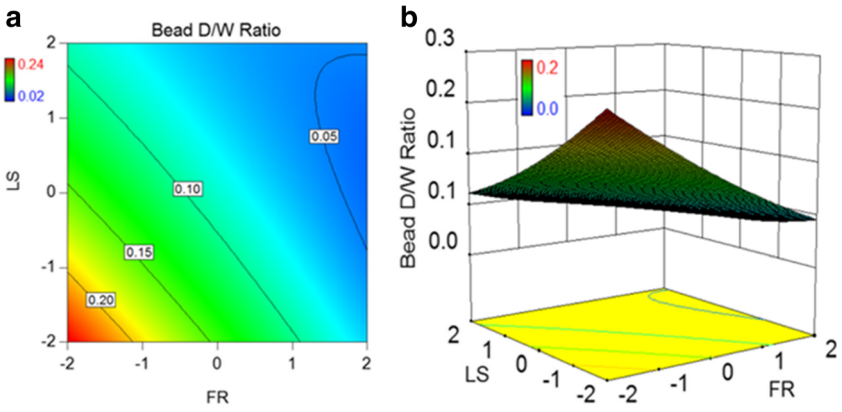

Fig. 10 **a** 2D contour plot and **b** 3D response surface plot show the interaction effect of powder flow rate (*FR*) and laser speed (*LS*) on the depth of penetration-to-bead width ratio

In Fig. 7, the curves AA (FR), BB (LP), DD (LS), and EE (CTD) have large curvatures, which indicates that the related process parameters are very sensitive to the respective response in their respective model. The curve CC (FL) shows a relatively flat line in Fig. 7a–c indicating that the FL is truly insensitive to its respective responses. The curve EE also shows a flat line in Fig. 7b, indicating its (factor CTD) insensitivity to the D/W ratio.

Figure 7 a and b shows that the FR curve AA has the highest negative effect on the bead W/H and D/W ratios compared to any other factors. However, the FR has the highest positive effect on the bead wetting angle, as shown in Fig. 7c, which is logical. The AA curve in Fig. 7d shows that FR has a mild positive effect on the bead microhardness.

Figure 7b shows that the LP curve BB has the highest positive effect on the D/W ratio, which is realistic as more laser power will increase the penetration depth. The LP (curve BB) also shows the mild effect on the bead W/H ratio (Fig. 7a) and a mildly negative effect on the bead wetting angle (Fig. 7c). Curve BB has a shallow convex shape for the bead microhardness in Fig. 7d, so its influence is situation dependent.

The curve DD in Fig. 7d shows that the LS has a very positive effect on the bead microhardness. Interestingly, this finding is strongly supported by the earlier study done by the current authors [21, 33] using different analysis techniques. It was found that at a higher laser speed, a higher residual stress generated due to higher cooling rate during solidification of the laser-cladded sample. Consequently, a very fine martensitic matrix along with eutectic delta ferrite and carbide phases (e.g., $Cr_{23}C_6$) contributed for the higher hardness in the bead zone [33].

The curve DD in Fig. 7a shows that the LS has a positive effect on the bead W/H ratio. However, it has a negative effect on the D/W ratio (Fig. 7b) and the bead wetting angle (Fig. 7c). On the other hand, it is observed that the FL curve CC does not show any significant effect on the bead geometry (W/H ratio, D/W ratio, and bead wetting angle), but there is a concave curve for the bead microhardness (Fig. 7d). Similar to the LP, this parameter's influence is situation dependent.

The curve EE shows that CTD has a positive effect on the bead W/H ratio (Fig. 7a), while a negative effect on the bead wetting angle (Fig. 7c). However, it does not show a signifi-

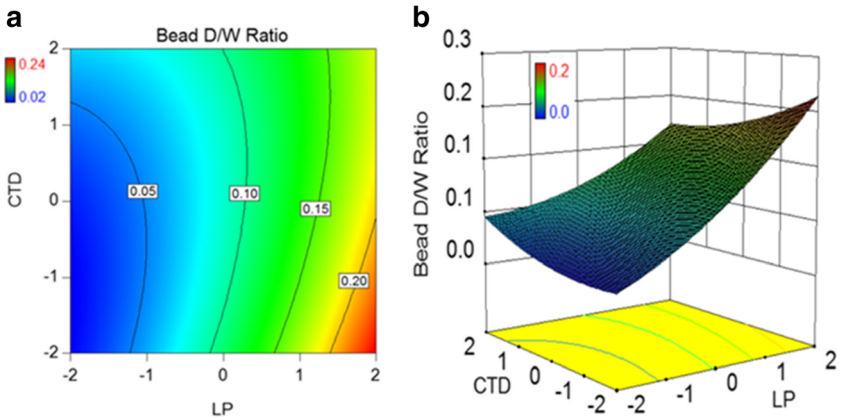

Fig. 11 **a** 2D contour plot and **b** 3D response surface plot show the interaction effect of laser power (*LP*) and contact tip to work distance (*CTD*) on the depth of penetration to bead width ratio

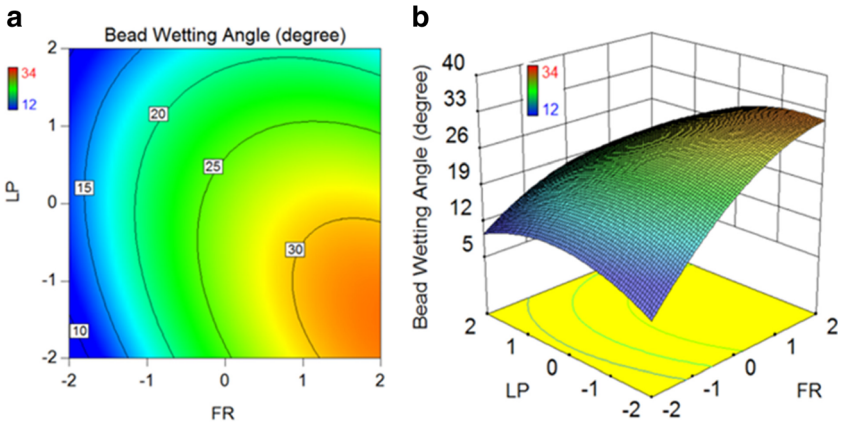

Fig. 12 **a** 2D contour plot and **b** 3D response surface plot show the interaction effect of powder flow rate (*FR*) and laser power (*LP*) on the bead wetting angle

cant effect on the D/W ratio despite showing both positive and negative effects on the bead microhardness. The trends observed in all those curves are elaborated in Section 3.2.3.

3.2.2 Two-factors interaction effect analyses

Selected two-factor interaction effects are depicted in the 2D contour plots and 3D surface mapping plots in Figs. 8, 9, 10, 11, 12, 13, 14, 15, 16, and 17. The plots are non-linear and asymmetric and include saddle surfaces. There is a strong interaction effect of FR and LS on the bead W/H ratio (Fig. 8) and a moderate interaction effect of FL and CTD on the same response output (Fig. 9). Both figures illustrate an asymmetric concave response surface. The FR influence on the D/W ratio depends on the LS (Fig. 10). Both the magnitude and direction are in variety, as can be seen by the surface twist. The influence of the LP has also impacted the CTD values. The smaller the CTD value (a shorter distance) and the higher the power, the greater the D/W ratio, which is realistic. The interaction effects of the FR and LP and FL and CTD, on the bead wetting angle, generates convex surfaces (Figs. 12 and 13). Noticeable asymmetry can be observed with the FR and LP relationships.

The two-factor relationships for the microhardness are more complex. In Fig. 14, at the minimum FR and LS values, the lowest hardness results. Changing either or both increases the hardness. A saddle surface is generated when evaluating the LP and FL and the LP and CTD (Figs. 15 and 16). Figure 15 shows that bead microhardness increases at a higher FL with a medium LP setting and decreases at the interaction of both at their lower values, while Fig. 16 shows that microhardness increases at both extremely high and extremely low value of LP and CTD compared to the average central value. These surfaces clearly illustrate the difficulty in developing predictive models that can capture the process variation effects. For the FL and CTD interaction, a concave surface, with limited asymmetry, is generated. The contours of the predicted response are almost concentric circles. The predicted bead microhardness is found unchanged in an increasing manner as the interaction of the FL and CTD is rotated about the center (0,0). This rotatability is a rational basis for the selection of a response surface design [3].

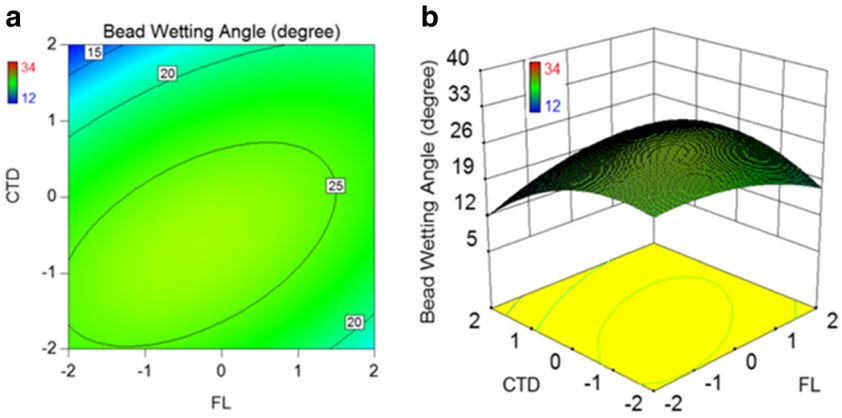

Fig. 13 **a** 2D contour plot and **b** 3D response surface plot show the interaction effect of focal length of the lens (*FL*) and contact tip to work distance (*CTD*) on the bead wetting angle

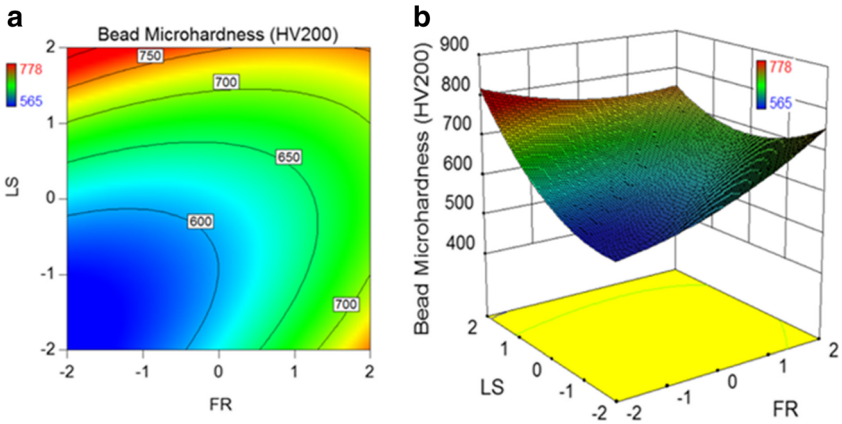

Fig. 14 **a** 2D contour plot and **b** 3D response surface plot show the interaction effect of powder flow rate (*FR*) and laser speed (*LS*) on the bead microhardness

3.2.3 Quadratic effect analyses

The perturbation plots, as well as the contour and surface plots, are used to portray the actual quadratic effect by adding significance level of curvature on the individual curve and 2FI surfaces.

As can be seen in Fig. 7d, the curve EE (relating to factor CTD) has the highest curvature compare to all other factors on the respective responses showing the highest quadratic effect of CTD on the bead microhardness. On the other hand, the curve CC (relating to factor FL) is found to be relatively flat in Fig. 7a–c, which indicates that the FL has the least quadratic effect on the D/W ratio (Fig. 7b), W/H ratio (Fig. 7a), and bead wetting angle (Fig. 7c). Interestingly, all factors show a concave relationship with the bead W/H ratio (Fig. 7a), a convex relationship with the bead wetting angle (Fig. 7c), a combination of concave and convex relationship with the bead microhardness (Fig. 7d), and a combination of concave, convex, and almost flat (least quadratic effect), relationship with the D/W ratio (Fig. 7b). These trends are summarized in Table 7.

Similarly, when those quadratic effects are applied on the 2D contour plots and 3D surface plots, they may create a minimum, maximum, or a saddle point response surface. However, sometimes there are variations from the pure minimum, maximum, or saddle point response surfaces. In those cases, quadratic effect indicates a rising ridge or a falling ridge systems [34]. Figures 8, 9, and 17 illustrate a response surface with a minimum, Fig. 13 shows a maximum, and Figs. 15 and 16 illustrate surfaces with a saddle point. On the other hand, Figs, 10, 11, 12, and 14 deviate from the pure minimum or maximum surface, thus creating a falling ridge (Fig. 10) and rising ridge systems (Figs. 11, 12, and 14). These plot shapes are summarized in Table 8.

In all cases, the factors with high quadratic effect facilitate to locate the optimum predicted response or a stationary point with reasonable precision by characterizing the shape of the surface [3].

3.3 Process planning challenges

The complex, highly coupled characteristics associated with laser cladding have been highlighted in these predictive modeling analyses. The parameters that have a great influence

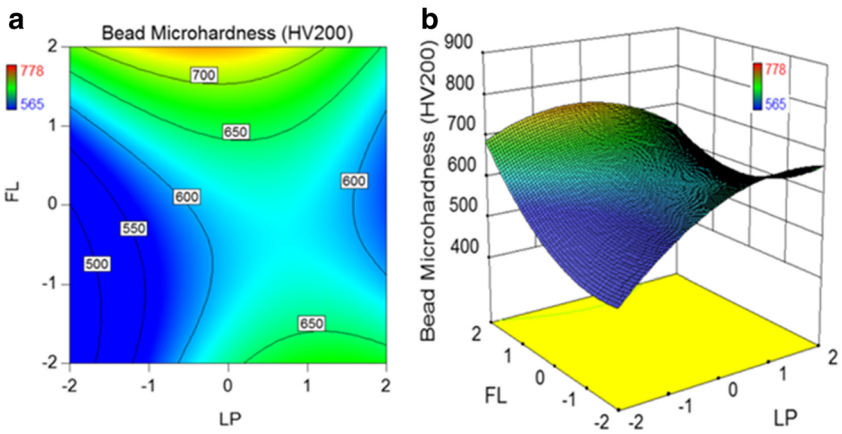

Fig. 15 **a** 2D contour plot and **b** 3D response surface plot show the interaction effect of laser powder (*LP*) and focal length of the lens (*FL*) on the bead microhardness

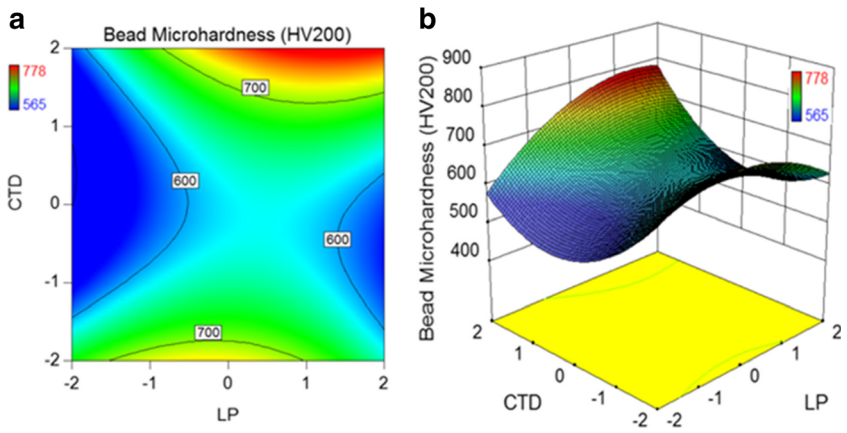

Fig. 16 **a** 2D contour plot and **b** 3D response surface plot show the interaction effect of laser powder (*LP*) and contact tip to work distance (*CTD*) on the bead microhardness

on hardness have a lesser influence on the bead geometry, but all process parameters and several interactions are statistically significant. For example, if a process planner desired a 4 ± .1 mm bead width, with a minimum 0.7 mm bead height (features readily measurable for real-time feedback control), there is a wide array of process settings that can generate the required geometry. There are five inputs (four inputs are controllable, and one input is a setup parameter—the focal length) and three geometric output requirements. A sample of experimental settings that provide a geometric solution is shown in Table 9. It can be seen that there is a wide range of settings for each parameter.

However, from Eq. 6, the predicted bead hardness indicates that the hardness can vary between 616 and 757 HV200. This is a wide range of hardness values, and as there is an empirical relationship between hardness and ultimate tensile strength [22, 23, 35], there will be an impact on the mechanical properties of the clad. Establishing a threshold range for the desired hardness as well as the bead aspect ratios can provide constraints assist in selecting optimal settings that will result in desired geometry and functional characteristics.

4 Summary and conclusions

Selecting process settings to fabricate a laser clad bead, which has the desired geometry and mechanical properties, is a challenge. Consequently, a structured experimental approach was taken to investigate relationships and develop predictive models. To minimize experiments, a RSM study, using a CCD, for predicting bead geometry and bead microhardness characteristics for laser-cladded AISI 420 stainless steel single-track beads has revealed important relationships among the process parameters and the response outputs. Predictive models for the bead geometry (W/H ratio, D/W ratio, and bead wetting angle) and the bead microhardness are developed using the RSM regression analysis. The statistical significance of the individual process parameters, their two-factor interactions, and quadratic effects on the predicted response output are analyzed using the *F*-statistics, perturbation plots, 2D contour plots, and 3D surface plots. While *F*-statistics can identify the relative importance of the factors over the others on the predictive response, it cannot quantify the effects whether happened in a positive way or negative way. That limitation

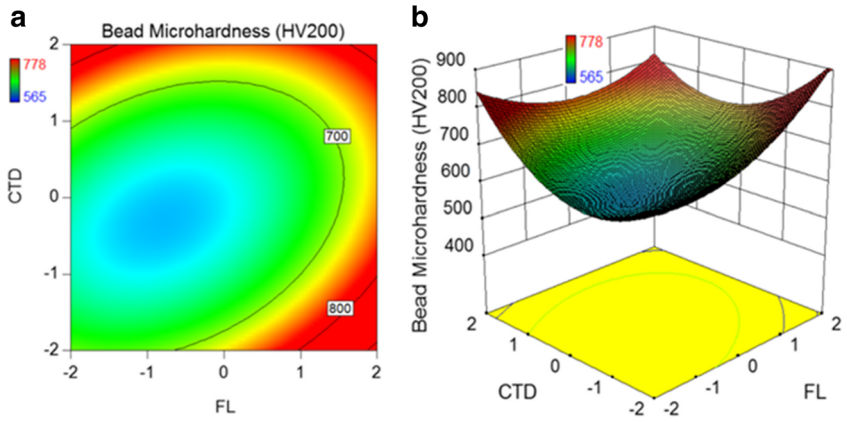

Fig. 17 **a** 2D contour plot and **b** 3D response surface plot show the interaction effect of focal length of lens (*FL*) and contact tip to workpiece distance (*CTD*) on the bead microhardness

Table 7 Quadratic effect of process parameters on the bead characteristics

Process parameter	Related curve (Fig. 7)	Quadratic/ curvature (type, magnitude and slope) effect of process parameters on the bead characteristics			
		W/H ratio	D/W ratio	Wetting angle	Microhardness
FR	AA	C, Steep, −ve	Flat, Steep, −ve	VX, Steep, +ve	C, Shallow, +ve
LP	BB	C, Shallow, +ve	Flat, Steep, +ve	VX, Shallow, −ve	VX, Steep, +ve
FL	CC	C, Shallow, ±ve	VX, Shallow, ±ve	VX, Shallow, ±ve	C, Steep, +ve
LS	DD	C, Shallow, +ve	Flat, Steep, −ve	VX, Shallow, −ve	C, Steep, +ve
CTD	EE	C, Shallow, +ve	C, Shallow, ±ve	VX, Shallow, −ve	C, Steep, ±ve

C concave, *VX* convex, *+ve* positive, *−ve* negative, *±ve* positive/negative

of *F*-statistics can overcome by using perturbation plots. Perturbation plots can identify and quantify both the positive and negative effects of the linear factors on the respective predictive responses. However, a perturbation plot cannot show the interaction effect of the process parameters. 2D contour plots and 3D surface plots are employed to interpret the two-factor interaction effect keeping the other factors constant at reference level (coded 0), where the quadratic effects are reflected indicating the trends of curvature in the response values.

Based on the performed RSM multiple regression and ANOVA results the following conclusions can be drawn:

1. The RSM analysis with a CCD approach is found to be a very efficient methodology to develop a robust prediction model using multiple process parameters for the bead aspect ratios, wetting angle, and the bead microhardness.
2. The ANOVA results for the R-squared values, the predicted R-Squared, and adjusted R-square values show that the regression models are significantly fitted with the data for a wide range of process settings. Therefore, a general model with a database of coefficients can be used to select process parameters and/or predict results for the bead geometry characteristics and hardness with confidence.
3. The FR and LS are found to be the most significant process parameters on the bead geometry characteristics and the bead microhardness, respectively. Consequently, selecting process parameters to generate a bead geometry only may lead to undesirable hardness results.
4. The interaction of the FR and LS has the most significant effect on the bead aspect ratios and bead microhardness, while the interaction of the FR and LP has the most significant effect on the bead wetting angle. The interaction of the FR and FL has the most insignificant effect on the predicted bead geometry. However, this interaction factor is still significant for the bead microhardness. The interaction of the LP and LS had the most insignificant effect on the predicted bead microhardness though this factor is still significant for the bead aspect ratio. Therefore, a very intriguing and complex relationship is observed within the process parameters and their interactions on the predicted bead geometry and bead microhardness. This analysis illustrates the difficulty in generating optimal solutions.

Table 8 Quadratic effect of two-factor interactions on the bead characteristics

Two-factor interactions	Quadratic/ curvature (type, magnitude) effect of two-factor interactions on the bead characteristics			
	W/H ratio	D/W ratio	Wetting angle	Microhardness
FR*LS	Concave, Minimum (Fig. 8)	Concave, Falling Ridge (Fig. 10)	–	Concave, Rising Ridge (Fig. 14)
FL*CTD	Concave, Minimum (Fig. 9)	–	Convex, Maximum (Fig. 13)	Convex, Minimum (Fig. 17)
LP*CTD	–	Concave, Rising Ridge (Fig. 11)	–	Twist, Saddle (Fig. 16)
FR*LP	–	–	Convex, Rising Ridge (Fig. 12)	–
LP*FL	–	–	–	Twist, Saddle (Fig. 15)

Table 9 Experimental settings and measured bead geometry for a 4 ± 0.1 mm bead width

FR	LP	FL	LS	CTD	Width (mm)	Height (mm)	Depth (mm)	W/H Ratio	D/W Ratio
25	3	390	12.5	22	3.9	0.9	0.4	4.33	0.10
25	2	410	7.5	24	3.9	0.9	0.3	4.33	0.08
20	2.5	400	15	23	4.0	0.7	0.2	5.71	0.05
15	2	410	7.5	22	4.0	0.8	0.5	5.00	0.13
20	2.5	400	10	25	4.0	0.8	0.4	5.00	0.10
20	2.5	400	10	23	4.1	1.1	0.3	3.73	0.07
				Average	4.0	0.8	0.3	4.68	0.09

FR powder feed rate, *LP* laser power, *LS* laser speed, *CTD* contact tip to workpiece distance, *FL* focal length of Lens, *W/H* width-to-height ratio, *D/W* depth of penetration-to-width ratio

5. The CTD has the highest quadratic effect on the bead microhardness followed by LS. The FR has the highest quadratic effect on the bead geometry despite having the least effect on the bead microhardness. The FL has the least quadratic effect on the responses except for the bead microhardness. The quadratic effects of those process parameters add significant curvature on the contour plots as well as identify a minimum, maximum, or a saddle point and ridge (rising ridge or a falling ridge) systems on the response surfaces of their respective 2D contour plots and 3D surface plots; therefore, simplified and linearized models cannot effectively predict solutions unless the range of process settings is narrow.
6. The 83% of the predicted response of the bead aspect ratios are found to be within ±10% error. However, 100% of the predicted responses for the bead microhardness are found to be within the ±4% error against the actual microhardness. Hence, these predictive model structures are found to be representative for a wide range of settings for laser cladding of AISI 420 stainless steel.
7. Due to the observed non-linear results, more experimental data needs to be collected to expand the models for overlapping and stacked beads for the laser cladding process.

This research will be expanded upon using the experimental approaches described in this work to consider evaluating the hardness and geometric characteristics for overlapping and multi-layer deposition scenarios. Also, the influence of the process parameters on the resultant residual stresses will be analyzed. This research will provide a foundation for optimization models for process planners to develop an optimal fabrication strategy.

Nomenclature

2D	2 Dimensional
2FI	2 Factor Interaction
3D	3 Dimensional
ANOVA	Analysis Of Variance
CCD	Central Composite Design
CTD	Contact Tip toWorkpiece Distance
D/W	Depth of Penetration to Bead Width Ratio
DF	Degree of Freedom
FL	Focal Length of Lens
FP	Focal Position of a laser beam
FR	Powder Feed Rate
HV	Hardness (Vickers Microhardness)
LC	Laser Cladding
LP	Laser Power
LPS	Laser Pulse Shape
LS	Laser Speed
MS	Mean Squares
PFA	Powder Feed Angle
PFP	Powder Feed Position
RSM	Response Surface Methodology
SD	Spot Diameter
SGT	Shielding Gas Type
SOD	Stand-Off Distance
SS	Sum of Squares
W/H	Bead Width to Height Ratio

Acknowledgments This research is funded by the Ontario Center of Excellence Collaborative Research program, Natural Sciences and Engineering Research Council of Canada through the Discovery Grant, and MITACs. The authors would like to thank the laser cladding industry sponsor and Camufacturing Solutions Inc. for the partial funding and resources they have provided for this research project.

References

1. Lepski D, Bruckner F (2009) Laser cladding. In *The Theory of Laser Materials Processing*, edited by John Dowden, online, 119: 235–79. Springer Netherlands. doi:10.2351/1.521888
2. Farahmand P, and Kovacevic R (2014) Parametric study and multi-criteria optimization in laser cladding by a high power direct diode

laser. Lasers Manuf Mater Process, 1–20. doi:10.1007/s40516-014-0001-0
3. Montgomery DC (2012) Design and Analysis of Experiments. 8th Ed., Wiley, pp 478-498. doi:10.1198/tech.2006.s372
4. Urbanic RJ, Hedrick RW, Burford CG (2017) A process planning framework and virtual representation for bead-based additive manufacturing processes. Int J Adv Manuf Technol 90(1–4):361–376. doi:10.1007/s00170-016-9392-8
5. Sun Y, Hao M (2012) Statistical analysis and optimization of process parameters in Ti6Al4V laser cladding using Nd: YAG laser. *Opt Lasers Eng* 50(7). Elsevier):985–995. doi:10.1016/j.optlaseng.2012.01.018
6. Saqib SM, Urbanic RJ, Aggarwal K (2014) Analysis of laser cladding bead morphology for developing additive manufacturing travel paths. *Procedia CIRP* 17. Elsevier B.V.:824–829. doi:10.1016/j.procir.2014.01.098
7. Benyounis KY, Olabi AG (2008) Optimization of different welding processes using statistical and numerical approaches—a reference guide. Adv Eng Softw 39(6):483–496. doi:10.1016/j.advengsoft.2007.03.012
8. Urbanic RJ, Saqib SM, Aggarwal K (2016) Using predictive modeling and classification methods for single and overlapping bead laser cladding to understand bead geometry to process parameter relationships. J Manuf Sci Eng 138(5):51012. doi:10.1115/1.4032117
9. Onwubolu GC, Davim JP, Oliveira C, Cardoso A (2007) Prediction of clad angle in laser cladding by powder using response surface methodology and scatter search. Opt Laser Technol 39(6):1130–1134. doi:10.1016/j.optlastec.2006.09.008
10. Liu S, Kovacevic R (2014) Statistical analysis and optimization of processing parameters in high-power direct diode laser cladding. Int J Adv Manuf Technol 74(5–8):867–878. doi:10.1007/s00170-014-6041-y
11. Aggarwal K (2014) investigation of laser clad bead geometry to process parameter settings for effective parameter selection, simulation, and Optimization.MASc thesis, University of Windsor
12. Aggarwal K, Urbanic RJ, Aggarwal L (2014) A methodology for investigating and modelling laser clad bead geometry and process parameter relationships. SAE Int 7(2):269–279
13. Mondal S, Paul CP, Kukreja LM, Bandyopadhyay A, Pal PK (2012) Application of Taguchi-based gray relational analysis for evaluating the optimal laser cladding parameters for AISI1040 steel plane surface. Int J Adv Manuf Technol 66(1–4):91–96. doi:10.1007/s00170-012-4308-8
14. Ituarte IF, Coatanea E, Salmi M, Tuomi J, Partanen J (2015) Additive manufacturing in production: a study case applying technical requirements. *Phys Procedia* 78 (august). Elsevier B.V.:357–366. doi:10.1016/j.phpro.2015.11.050
15. Majumdar JD, Manna I (2011) Laser material processing. Int Mater Rev 56(5/6):341–388. doi:10.1179/1743280411Y.0000000003
16. Zhu Z, Dhokia VG, Nassehi A, Newman ST (2013) A review of hybrid manufacturing processes—state of the art and future perspectives. Int J Comput Integr Manuf 26(7):596–615. doi:10.1080/0951192X.2012.749530
17. Lee HK (2008) Effects of the cladding parameters on the deposition efficiency in pulsed Nd: YAG laser cladding. J Mater Process Technol 202(1–3):321–327. doi:10.1016/j.jmatprotec.2007.09.024
18. Graf B, Ammer S, Gumenyuk A, Rethmeier M (2013) Design of experiments for laser metal deposition in maintenance, repair and overhaul applications. *Procedia CIRP* 11. Elsevier B.V.:245–248. doi:10.1016/j.procir.2013.07.031
19. Alam MK, Nazemi N, Urbanic RJ, Saqib SM, Edrisy A (2017) Investigating process parameters and microhardness predictive modeling approaches for single bead 420 stainless steel laser cladding. SAE Int. doi:10.4271/2017-01-0283
20. Baghjari SH, Mousavi SA (2013) Effects of pulsed Nd:YAG laser welding parameters and subsequent post-weld heat treatment on microstructure and hardness of AISI 420 stainless steel. Mater Des 43:1–9. doi:10.1016/j.matdes.2012.06.027
21. Alam MK, Urbanic RJ, Saqib SM, Edrisy A (2015) Effect of process parameters on the microstructural evolutions of laser cladded 420 martensitic stainless steel. In: Materials science and technology conference proceedings (MS&T15), October 4–8. Columbus, Ohio, USA, pp 35–54
22. Zhang P, Li SX, Zhang ZF (2011) General relationship between strength and hardness. Mater Sci Eng A 529:62–73. doi:10.1016/j.msea.2011.08.061
23. Datsko J, Hartwig L, Mcclory B (2001) On the tensile strength and hardness relation for metals. J Mater Eng Perform 10:718–722. doi:10.1361/105994901770344601
24. Saqib SM (2016) Experimental investigation of laser cladding bead morphology and process parameter relationship for additive manufacturing process characterization - Ph.D. dissertation. University of Windsor
25. Weidmann E (2005) Struers application notes—metallographic preparation of stainless steel. Copenhagen: Struers A/S. Doi:01.05 / 62140005
26. Nazemi N, Urbanic RJ, Alam MK (2017) Hardness and residual stress modeling of powder injection laser cladding of P420 coating on AISI 1018 substrate. Int J Adv Manuf Technol. doi:10.1007/s00170-017-0760-9
27. Nazemi N, Urbanic RJ (2016) A finite element analysis for thermal analysis of laser cladding of mild steel with P420 steel powder. In: Proceedings of the ASME 2016 international mechanical engineering congress and exposition IMECE2016 - November 11–17. Phoenix, Arizona, USA, pp 1–10
28. Nazemi N, Alam MK, Urbanic RJ, Saquib SM, Edrisy A (2017) A hardness study on laser cladded surfaces for a selected bead overlap conditions. SAE Int. doi:10.4271/2017-01-0285
29. Toyserkani E, Khajepour A, Corbin S (2004) 3-D finite element modeling of laser cladding by powder injection: effects of laser pulse shaping on the process. Opt Lasers Eng 41(6):849–867. doi:10.1016/S0143-8166(03)00063-0
30. Fu Y, Loredo A, Martin B, Vannes AB (2002) A theoretical model for laser and powder particles interaction during laser cladding. J Mater Process Technol 128(1–3):106–112. doi:10.1016/S0924-0136(02)00433-8
31. Anderson MJ, Whitcomb PJ, Kraber SL, Adams WF (2016) Handbook for Experimenters. Stat-Ease, Inc., Minneapolis, MN
32. Epps JA (2000) Compatibility of a test for moisture-induced damage with superpave volumetric mix design - NCHRP Report 444, National Cooperative Highway Research Program. National Academy Press, Washington D. C
33. Alam MK, Edrisy A, Urbanic RJ, Pineault J (2017) Microhardness and stress analysis of laser-cladded AISI 420 martensitic stainless steel. J Mater Eng Perform. doi:10.1007/s11665-017-2541-x
34. NIST/SEMATECH e-Handbook of Engineering Statistics (2013), http://www.itl.nist.gov/div898/handbook/pri/section3/pri336.htm, access date 09.02.2017
35. Gasko M, Rosenberg G (2011) Correlation between hardness and tensile properties in ultra-high strength dual phase steels–short communication. Mater Eng 18:155–159